TOWARD AN EMPIRICALLY-BASED PARAMETRIC EXPLOSION SPECTRAL MODEL

Sean R. Ford[1], William R. Walter[1], Stan D. Ruppert[1], Eric Matzel[1], Terri F. Hauk[1], and Rengin Gok[1]

Lawrence Livermore National Laboratory[1]

Sponsored by the National Nuclear Security Administration

Award No. DE-AC52-07NA27344/LL08-Parametrics-NDD02[1]

ABSTRACT

Small underground nuclear explosions need to be confidently detected and identified in regions of the world where they have never occurred. We are developing a parametric model of the nuclear explosion seismic source spectrum derived from regional phases (*Pn, Pg, Sn, and Lg*) that is compatible with earthquake-based geometrical spreading and attenuation. Earthquake spectra are fit with a generalized version of the Brune spectrum, which is a three-parameter model that describes the long-period level, corner-frequency, and spectral slope at high frequencies. These parameters are then correlated with near-source geology and containment conditions. There is a correlation of high gas-porosity (low strength) with increased spectral slope. However, there are trade-offs between the slope and corner-frequency, which we try to independently constrain using Mueller-Murphy relations and coda-ratio techniques. The relationship between the parametric equations and the geologic and containment conditions will assist in our physical understanding of the nuclear explosion source. The achievable goal of our parametric model development is to be able to predict observed local and regional distance seismic amplitudes for event identification and yield determination in regions with incomplete or no prior history of underground nuclear testing.

OBJECTIVES

We aim to develop a practical explosion source parametric spectral model, based on all available data, that describes nuclear explosion *P*- and *S*-wave source spectra for a variety of geologic and containment conditions. This approach follows the simple earthquake parametric spectral model based on Brune (1970), which is used for the MDAC approach (Walter and Taylor, 2002) to improve earthquake/explosion discrimination. In regions without prior explosions, the parametric model could be combined with earthquake-derived path corrections to predict explosion regional phase amplitudes, improve discriminants such as *P*/*S* ratios, and support identification procedures (e.g., Event Classification Matrix, [ECM]) that explicitly need to use explosion discriminant probability density functions.

It is well known that depth and near-source material properties can affect seismic estimates of explosion yield, and prior work at the Nevada Test Site (NTS) (e.g., Walter et al., 1995) has found that explosions in weak materials have lower corner frequencies and steeper spectral fall-offs for *P*-waves than is predicted by the standard Mueller and Murphy (1971) model. As part of this research, we hope to quantify these effects as a function of frequency and wave type. Additionally, many of the most effective regional discriminants (high-frequency *P*/*S* ratios) make use of *S*-waves, as do *S*-wave coda yield estimation techniques, yet there remain many questions about how to predict explosion *S*-wave amplitudes. The development of a combined *P*- and *S*-wave spectral model consistent with observed regional *P*-and *S*-wave data is a goal of this work.

RESEARCH ACCOMPLISHED

Introduction

In previous work that looked at low to high frequency ratios of regional phase (e.g., *Pn*, *Pg*, *Lg*) amplitudes to separate explosions from earthquakes at NTS, Walter et al. (1995) noted that the results showed a strong dependence on the source media properties. Nuclear tests in weak and/or high gas porosity media tended to have higher values and discriminate better from earthquakes than explosions in stronger and/or lower gas porosity media.

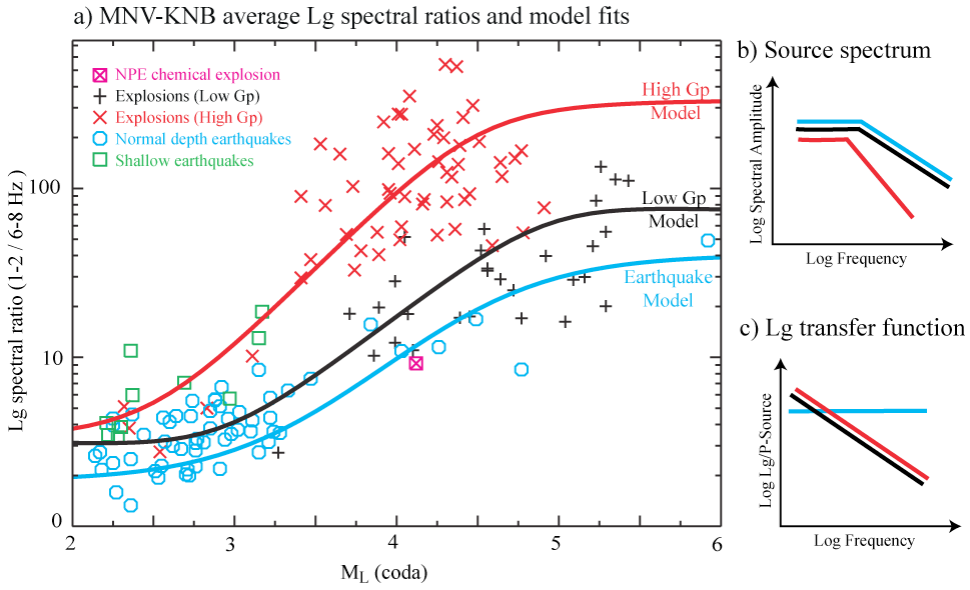

Figure 1. Simple first-order source model fits to low to high frequency spectral ratios of *Lg* amplitudes from Walter et al. (1995, Figure 8). Earthquake displacement spectra are fit with the Brune (1970) model (blue line), which is constant at low frequencies and falls off above a corner frequency as f^{-2}. Explosions are fit with two extremes of the Denny and Goodman (1990) model in order to investigate explosion dependence on emplacement material (namely, gas porosity [*Gp*]). The 'Low *Gp*' model (black line) has an effective fall-off similar to the earthquake model. The 'High *Gp*' model (red line) has a greater fall-off of f^{-3}.

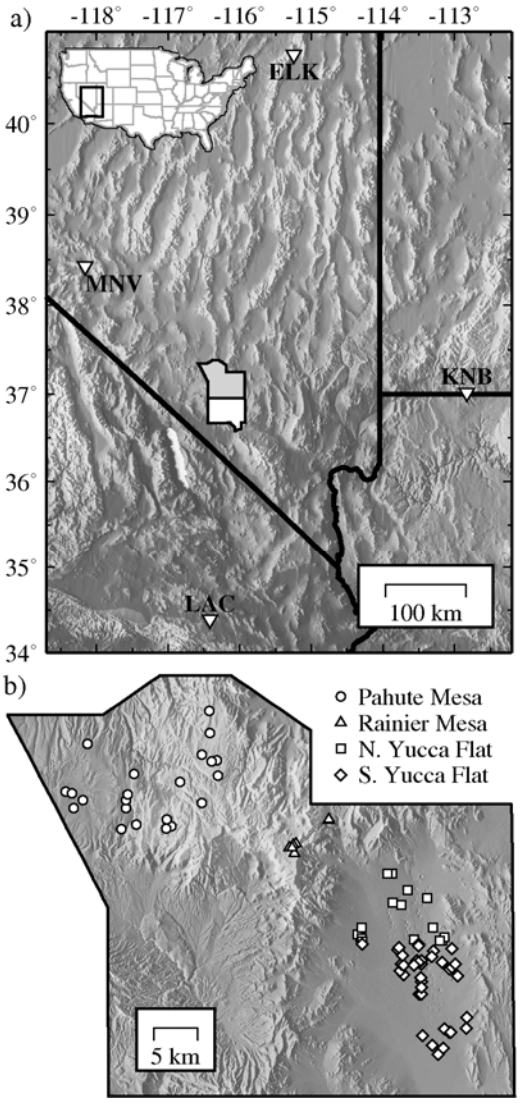

Figure 2. a) Regional map of stations used in the analysis. The location of the map within the continental US is given by the inset map. The NTS is outlined and the shaded section is shown in (b). b) Map of the northern NTS with explosion locations and Vergino and Mensing (1990) area designations.

For example, in Figure 1 the ratio of the *Lg* amplitude at 1–2 Hz compared with the amplitude at 6–8 Hz is shown as a function of magnitude. The earthquakes (blue circles and green squares) show the expected trend with magnitude going from a low value for small events when the corner frequency is above 8 Hz and both measurements are on the constant part of the source spectra that is proportional to moment. For large magnitudes, the source corner frequency drops below 1 Hz and then both measures are on the part of the source spectra that decays with frequency as f^{-2}, resulting in high spectral ratio values. As magnitude increases, the earthquakes follow a sigmoid curve as shown by the blue line, which is based on the Brune (1970) model. The explosions are split into two categories based on the source media, a high gas porosity (*Gp*) and low strength (defined as $\rho\alpha^2$, where ρ is density and α is the local compressional wave speed) group (red x) and low *Gp* high strength group (black crosses), and a clear difference between the two can be seen. In fact, the low *Gp* explosions reach spectral ratio values that imply much steeper falloff than f^{-2}.

To fit the explosion data, we used two extremes of the Denny and Goodman explosion model (1990), which has two corner frequencies. In the low *Gp* case we allowed the second corner to be at a higher frequency than the range of interest, giving an effective f^{-2} falloff. In the high *Gp* case we forced the corners to be the same, giving an f^{-3} falloff. In both cases we used the observed 3 Hz corner frequency of the 1993 Non-Proliferation Experiment (NPE), a kiloton chemical explosion and assumed the corner frequency scales with the cube root of M_L(coda). Given that a pure explosion should not generate *S*-waves, one way to think about the *Lg* spectral ratio is as the product of the *P*-wave source ratio and a transfer function ratio, where the transfer function is a representation of how efficiently the source generated *P*-waves are converted (by whatever means) into *S*-waves. We estimated the transfer function ratio as a function of frequency as shown in Figure 1, and then multiplied the *P*-wave based Denny-Goodman model curves by these factors and then compared them to the *Lg* spectral ratio in Figure 1. The result is a fairly reasonable first order fit to the data. Interestingly, since the explosion *Lg* transfer functions are larger than those for the earthquakes, it shifts the explosion *Lg* spectral ratios to relatively higher values than for the earthquakes, improving the discrimination performance of *Lg* spectral ratios over those of *Pn* alone (Walter et al. 1995, Figure 7).

While in this case, the Denny and Goodman (1990) model provides a reasonable fit to these NTS data, it is not clear how we would make use of it in other regions. Furthermore the limitation of only two choices of high frequency fall-off does not capture the full range of the observations. To develop a practical parametric source spectral model we want to be able to tie parameters like low-frequency level, corner-frequency and fall-off rate to

Table 1. NTS regional attenuation and geometric spreading parameters.

Phase	η	r_0 (km)	Q_0	γ
Pn	1.1	0. 001	210	0. 65
Pg	0.5	1 00	190	0 .45
Lg	0.5	1 00	200	0 .54

measureable properties like yield, depth, and media properties such as gas porosity, water content, and strength. In the next section we take a more general approach to fitting the NTS explosion data with a simple spectral model parameterized by a long-period level, corner-frequency, and high-frequency roll-off. We then relate these parameters for *Pn* spectra to source and medium properties. In the future we will perform similar analyses for *Pg* and *Lg* spectra.

Data and Methods

We employ the NTS explosion dataset of Walter et al. (2004), specifically the raw spectra of that dataset. Waveforms are de-meaned, de-trended and instrument corrected to acceleration. The signal is windowed with a 5% cosine taper that starts before the pick, where the time before the pick is 5% of the total time window. The Fourier transform is calculated and displacement spectra are obtained via double integration in the frequency domain. Finally, the resultant amplitude spectra are interpolated and smoothed to obtain a sampling period of 0.05 $\log_{10}$ Hz.

Spectra of each seismic phase for each explosion are calculated from the recordings of stations of the Livermore NTS Network, ELK (Elko, NV), KNB (Kanab, UT), LAC (Landers, CA), and MNV (Mina, NV). The locations of these stations relative to the NTS are given in Figure 2. These spectra are then corrected for geometrical spreading and regional, frequency-dependent attenuation of the form $Q = Q_0 f^{\gamma}$, where Q_0 is Q at 1 Hz and γ is the power-law dependence on frequency, f. We employ the Street et al. (1975) parametric form of geometrical spreading,

$$G(r) = \begin{cases} r^{-1}, & r < r_0 \\ 1/r_0 (r_0/r)^{\eta}, & r \geq r_0 \end{cases}, \qquad (1)$$

where r_0 is the distance at which the spreading transitions from spherical- to a cylindrical-type spreading and η is the distance dependence. The attenuation and spreading model parameters for each seismic phase are given in Table 1.

We require three of the four stations listed above to have recorded an event with a signal-to-noise ratio greater than two. We also inspect each spectra for non-stationary noise at high-frequency (typically >9 Hz) due to multi-band recording problems and restrict spectral fitting to bands unaffected by problems. The spectra are jointly fit with a simple parametric form given by

$$S(f) = \frac{S_0}{1 + (f/f_c)^{\psi}}, \qquad (2)$$

in a least-squares inversion that also provides standard error for each parameter estimate. Equation (2) describes the

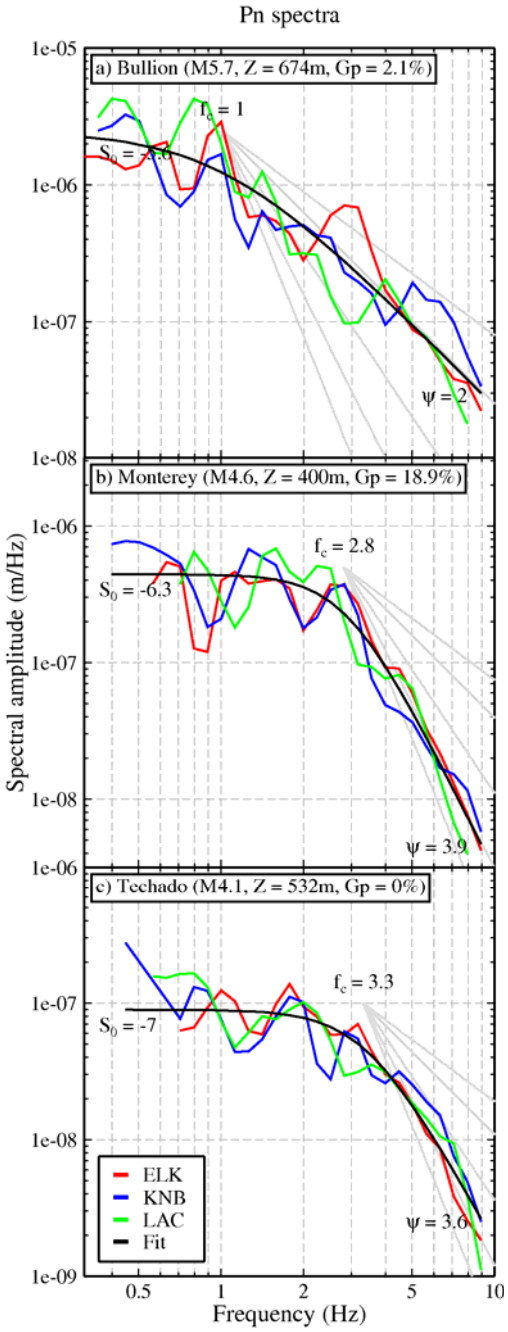

Figure 3. *Pn* spectra examples with the name, magnitude (where $M = m_b[Pn]$), depth (*Z*), and gas porosity (*Gp*) given in the subtitles. The long-period level (S_0), corner-frequency (f_c), and fall-off (ψ) are given in each plot, and the spectra are colored by station and the fit is shown in the legend in the lowermost plot. a) Spectra for an event with low *Gp* and ω^{-2} fall-off. b) Spectra for an event with high *Gp* and high fall-off. c) Spectra for an event with low *Gp* and high fall-off.

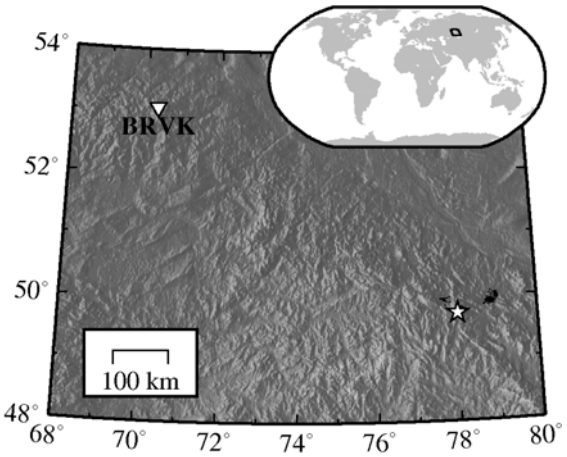

Figure 4. Regional map of station in Borovoye (BRVK) and recorded events in the archive (dots) along with the event shown in Figure 5 (star). The location of the map is given in the inset global map.

simplest behavior expected for seismic spectra. It has a constant level at low frequencies (S_0), which is proportional to static displacement, and falls off at high frequencies with a slope of $f^{-\psi}$ beyond a corner frequency f_c. Examples of the spectra and model fits are proportional to static displacement, and fall off at high frequencies with a slope of $f^{-\psi}$ beyond a corner frequency f_c. Examples of the spectra and model fits are given in Figure 3. BULLION (Figure 3a) is fit well with a standard f^{-2} (ψ=2) spectral fall-off, but MONTEREY (Figure 3b), detonated in weak material, requires a steeper fall-off where the best fit $\psi \approx 4$.

We plan to complement the NTS dataset with the Borovoye (BRV) archive that has recently been deglitched and response functions estimated (Richards and Kim, 2009). This archive could potentially provide 200 recordings of explosions at Semipalatinsk Test Site of the former Soviet Union (Figure 4). As an example, we plot the regional phase spectra of one of the explosions mapped in Figure 4 (shown by a star) in Figure 5. The attenuation and spreading model parameters used to correct these spectra are given in Table 2. The *Pn* and *Pg* spectra are fit with $\psi \approx 3$, whereas *Lg* fall-off is approximately $\psi \approx 2$.

The BRV regional seismic phase spectra, especially *Pn* and *Pg* (Figure 5a-b), show the trade-off in fitting the corner frequency and the roll-off. In this case a slightly smaller f_c would lead perhaps a more appropriate ψ of 2. Attempts to diminish this trade-off will be discussed in the next section.

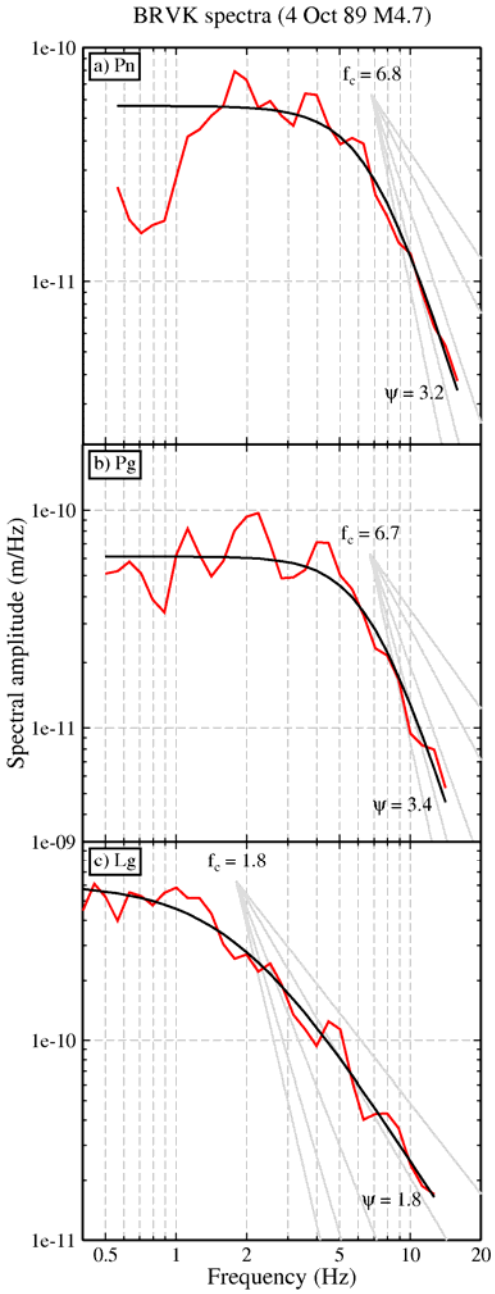

Figure 5. *Pn* spectra of example BRVK event (shown by star in Figure 4). Values given in each plot are defined in Figure 3.

Preliminary results

We present the results of fitting the *Pn* spectra for NTS explosions in Figure 6, where corner-frequency is plotted versus fall-off. There is a correlation between the two estimated parameters that is most probably related to the least-squares fitting of Equation (2) and not to any physical relationship. This trade-off can be seen graphically

Table 2. BRV regional attenuation and geometric spreading parameters

Phase	η	r_0 (km)	Q_0	γ
Pn	1.1	0.001	210	0.65
Pg	0.5	1.00	190	0.45
Lg	0.5	1.00	200	0.54

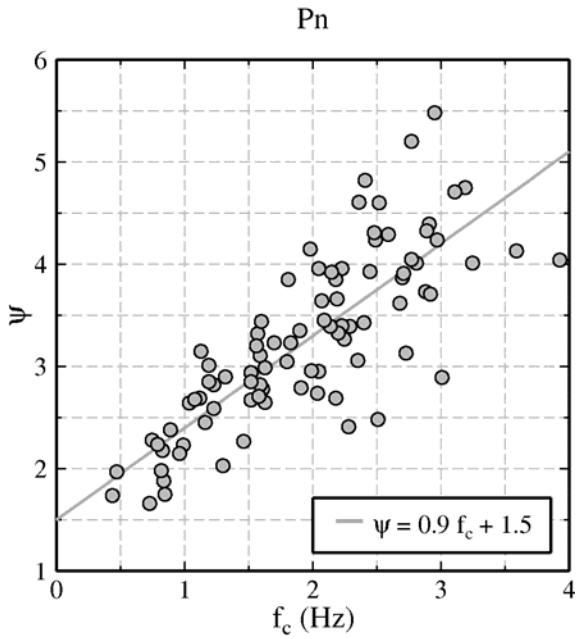

Figure 6. Correlation of estimated source parameters, corner-frequency (f_c) and fall-off (ψ) from Equation (2).

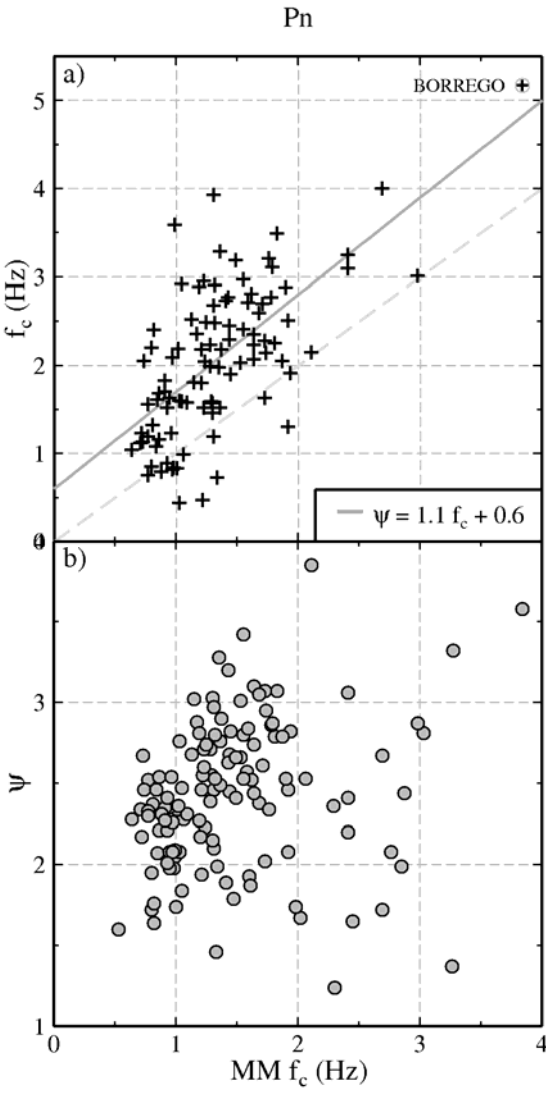

Figure 7. a) Corner-frequency (f_c) from the fits to Equation (2) compared with those predicted by Mueller and Murphy (1971), MM71 f_c. The linear relationship is given by the equation at the top of the plot and the slope is close to one. b) ψ obtained while fixing f_c in Equation (2) to the MM71 f_c. The correlation of the terms is reduced compared with Figure 6.

in the BRV spectra plotted in Figure 5. The trade-off could produce biased estimates of ψ, so we seek to constrain f_c in Equation (2) using the corner frequency predicted by Mueller and Murphy (1971) as parameterized by Stevens and Day (1985) for tuff/rhyolite. Figure 7a shows that the freely-fit f_c is well-correlated with the Mueller and Murphy (1971) predicted corner-frequency (MM f_c) and the slope is close to one. It can be made even closer by decreasing the reference elastic radius used to calculate the proportionality constant used in the Mueller and Murphy (1971) relationship. We set f_c = MM f_c in Equation (2) and estimate ψ. This new ψ is less correlated with MM f_c as shown in Figure 7b.

A least-squares regression of spectral fall-off (ψ) for *Gp* is given in Figure 8a, where the weights are given by the inverse variance of ψ estimated by the inversion. Figure 8b is the same, but uses the estimated ψ while fixing f_c as described previously. We also perform a comprehensive search for material property correlation with ψ, using several regressions on ψ for water content (S_W), gas porosity (*Gp*), density (ρ), compressional wave speed (α), compressional modulus ($\rho\alpha$), strength ($\rho\alpha^2$), depth, depth to water-table, and scaled depth-of-burial (sDOB = depth/yield$^{1/3}$). These geophysical parameters are taken from the database of Springer et al. (2002) and are reported to represent an integrated value over the source region. Yield was inferred from m_b(*Pn*) based on the Vergino and Mensing (1990) relationship at NTS. Using a step-wise regression criteria we found the most significant parameters in a linear regression model to be S_W, *Gp*, and sDOB.

We then perform a least-squares regression using these parameters weighted by the estimated inverse variance of ψ. The model is given by

$$\psi = 2.977 - 4.026Gp + 3.519S_w + 2.81\times10^{-3}\,sDOB\,. \qquad (3)$$

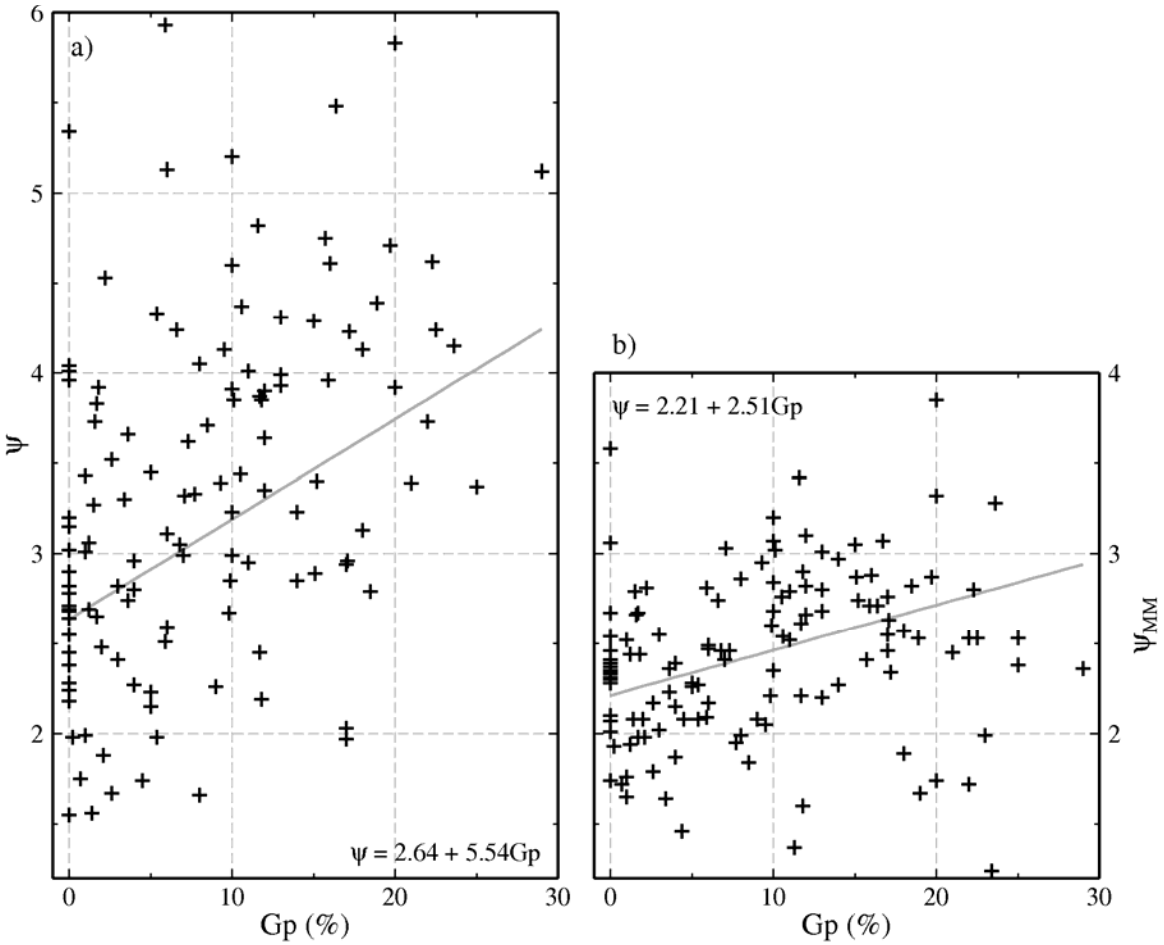

Figure 8. Fall-off (ψ) as a function of gas porosity (*Gp*) for a) unconstrained f_c and, b) f_c fixed to the MM71-predicted value. The best-fit relationship weighted by the inverse variance of the estimated ψ is given in the inset equation.

When we regress using ψ estimated while fixing f_c, we get a slightly different model given by

$$\psi = 1.823 + 0.433Gp + 1.710S_w + 2.21\times10^{-3}\,sDOB. \quad (4)$$

In new testing environments geophysical parameters such as gas porosity and water content may not be accessible. Using NTS geophysical data from Springer et al. (2002) we find that Gp is best approximated by ρ, α, and their interaction, $\rho\alpha$, also known as the compressional modulus. This relationship is given by

$$Gp = 1.266 - 5.437\times10^{-4}\rho - 3.776\times10^{-4}\alpha + 1.635\times10^{-7}\rho\alpha, \quad (5)$$

where is ρ is in kg/m^3 and α is in m/s.

CONCLUSIONS AND RECOMMENDATIONS

Our preliminary analysis of *Pn* spectra of NTS explosions shows that a simple spectral model with variable fall-off is appropriate, and the fall-off correlates well with material properties, gas porosity and water-content, and the scaled depth-of-burial. Corner-frequencies obtained with the variable fall-off model correlate with Mueller and Murphy (1971) corner-frequencies. If we use a smaller elastic radius than the one given for tuff, we believe we could match the trend of the Mueller-Murphy corner frequencies with a slope close to one.

Future Work

This initial *P*-wave spectral fitting focused on correlating material properties with the model parameters. We will perform similar analyses for NTS seismic phases, *Pg* and *Lg*, and compare the results with those presented above for *Pn*. We will make similar calculations for spectra at Borovoye. The comparison of seismic phases will allow for an examination of *P/S* scaling relationships, which can be compared with results from the Fisk (2007) study at NTS. The results of this study with a variable fall-off spectral model will be compared with other spectral models (e.g., Denny and Johnson [1991] and references therein). In addition, we will formally analyze the error and trade-offs in the estimated parameters of Equation (2).

REFERENCES

Baker, D., W.-Y. Kim, H. Patton, G. Randall, and P. Richards (2009). Improvements to a major digital archive of seismic waveforms from nuclear explosions: The Borovoye seismogram archive, in *Proceedings of the 2009 Monitoring Research Review: Ground-Based Nuclear Explosion Monitoring Technologies,* LA-UR-09-05276, Vol. 1, pp. 12–21.

Brune, J. N. (1970). Tectonic stress and the spectra of seismic shear waves from earthquakes, *J. Geophys. Res.* 75: 4997–5009.

Denny, M. D. and D. M. Goodman (1990). A case study of the seismic source function; SALMON and STERLING reevaluated, *J. Geophys. Res.* 95: 19705–19723.

Denny, M. D. and L. R. Johnson (1991). The explosion seismic source function: Models and scaling laws reviewed, in *Explosion Source Phenomenology*, eds. Taylor S. R. et al., AGU Monograph 65: 1–24.

Fisk, M. D. (2007). Corner frequency scaling of regional seismic phases for underground nuclear explosions at the Nevada Test Site, *Bull. Seismol. Soc. Am.* 97: 977–988.

Goldstein, P., S. P. Jarpe, K. M. Mayeda, and W. R. Walter (1994). Separation of source and propagation effects and regional distances, in *Proceedings of the Symposium on the Non-Proliferation Experiment: Results and Implications for Test Ban Treaties,* DOE-CONF-9404100, 6-272–6-276.

Mueller, C. S. and J. R. Murphy (1971). Seismic characteristics of underground nuclear detonations, Part I: Seismic spectrum scaling, *Bull. Seismol. Soc. Am.* 61: 1675–1692.

Stevens, J. L. and S. M. Day (1985). The physical basis of m_b:M_S and variable frequency magnitude methods for earthquake/explosion discrimination, *J. Geophys. Res.* 90: 3009–3020.

Street, R. L., R. B. Herrmann, and O. W. Nuttli (1975). Spectral characteristics of the Lg wave generated by central United States earthquakes, *Geophys. J. R. Astro.* 41: 51–63.

Vergino, E. S. and R. W. Mensing (1990). Yield estimation using regional mb(Pn), *Bull. Seismol. Soc. Am.* 80: 656–674.

Walter, W. R, K. D. Smith, J. L. O'Boyle, T. F. Hauk, F. Ryall, S. D. Ruppert, S. C. Myers, R. Abbot, and D. A. Dodge (2004). An assembled western United States dataset for regional seismic analysis, *Lawrence Livermore National Laboratory* document, UCRL-TR-206630.

Walter, W. R. and S. R. Taylor (2002). A revised magnitude and distance amplitude correction (MDAC2) procedure for regional seismic discriminants, *Lawrence Livermore National Laboratory* document, UCRL-ID-146882.

Walter, W. R., K. M. Mayeda, and H. J. Patton (1995). Phase and spectral ratio discrimination between NTS earthquakes and explosions, Part 1: Empirical observations, *Bull. Seimol. Soc. Am.* 85: 1050–1067.